INTERNATIONAL JOURNAL FOR NUMERICAL METHODS IN FLUIDS
Int. J. Numer. Meth. Fluids 2005; **48**:271–303
Published online 24 January 2005 in Wiley InterScience (www.interscience.wiley.com). DOI: 10.1002/fld.837

On the practical importance of the SSP property for Runge–Kutta time integrators for some common Godunov-type schemes

David I. Ketcheson*,† and Allen C. Robinson‡

Sandia National Laboratories, P.O. Box 5800, Albuquerque, NM 87185-0378, U.S.A.

SUMMARY

We investigate through analysis and computational experiment explicit second and third-order strong-stability preserving (SSP) Runge–Kutta time discretization methods in order to gain perspective on the practical necessity of the SSP property. We consider general theoretical SSP limits for these schemes and present a new optimal third-order low-storage SSP method that is SSP at a CFL number of 0.838. We compare results of practical preservation of the TVD property using SSP and non-SSP time integrators to integrate a class of semi-discrete Godunov-type spatial discretizations. Our examples involve numerical solutions to Burgers' equation and the Euler equations. We observe that 'well-designed' non-SSP and non-optimal SSP schemes with SSP coefficients less than one provide comparable stability when used with time steps below the standard CFL limit. Results using a third-order non-TVD CWENO scheme are also presented. We verify that the documented SSP methods with the number of stages greater than the order provide a useful enhanced stability region. We show by analysis and by numerical experiment that the non-oscillatory third-order reconstructions used in (Liu and Tadmor *Numer. Math.* 1998; **79**:397–425, Kurganov and Petrova *Numer. Math.* 2001; **88**:683–729) are in general only second- and first-order accurate, respectively. Copyright © 2005 John Wiley & Sons, Ltd.

KEY WORDS: strong stability preserving; total variation diminishing; Runge–Kutta methods; high-resolution; hyperbolic conservation laws; Godunov; central schemes; Riemann solvers

1. INTRODUCTION AND BACKGROUND

Many important problems in mathematical physics can be cast in a general conservation law form

$$\frac{\partial \mathbf{u}}{\partial t} + \frac{\partial \mathbf{F}(\mathbf{u})}{\partial x} = 0 \tag{1}$$

*Correspondence to: David I. Ketcheson, University of Washington, Applied Mathematics, Box 352420, Seattle, WA 98195-2420, U.S.A.
†E-mail: ketch@amath.washington.edu
‡E-mail: acrobin@sandia.gov

Contract/grant sponsor: United States Department of Energy; contract/grant number: DE-AC04-94AL85000

Received 3 March 2004
Revised 15 November 2004
Accepted 18 November 2004

where $\mathbf{u}$ is the vector of conserved variables and $\mathbf{F}(\mathbf{u})$ the flux function. The system is hyperbolic if the Jacobian matrix $\mathbf{A} = \partial\mathbf{F}/\partial\mathbf{u}$ has real eigenvalues and a complete set of eigenvectors. A method of lines approximation to this system results in a semi-discrete formulation

$$\frac{\partial \mathbf{u}}{\partial t} = \mathscr{L}(\mathbf{u}) \tag{2}$$

that may be advanced in time via an ordinary differential equation solver. Numerical time integration methods can be developed to satisfy requirements on temporal truncation error, dispersive properties (phase and group errors), numerical dissipation, and memory, depending on the particular application constraints that are considered to be most important. The work by Kennedy *et al.* [1] and Kennedy and Carpenter [2] provides a good overview of these technical issues. In general, a time marching method of accuracy compatible with the accuracy of the spatial discretization should be used to integrate Equation (2) forward in time.

It has been proposed that time integration methods that satisfy a strong-stability preserving (SSP) property are preferable for method of lines approaches to solving non-linear hyperbolic conservation laws [3–6]. SSP methods, also referred to as TVD time discretizations, are high-order time integration algorithms that preserve the strong stability properties of the first-order Euler time integrator. In this paper we focus on the SSP properties of Runge–Kutta methods.

SSPRK methods were first discussed by Shu and Osher [6]. Gottlieb and Shu derived optimal second-, third-, and fourth order SSPRK methods with the number of stages equal to the order of accuracy [3]. Spiteri and Ruuth have provided s-stage, p-order SSPRK methods where $s > p$ and have demonstrated the expanded stability regions of these schemes which are beneficial even after normalizing by cost [7, 8]. A concise summary of important SSP results is given by Shu [5].

Low-storage (LS) Runge–Kutta methods in conjunction with high-resolution spatial discretization schemes may be of particular interest for large scale applications. Williamson reviews LS methods of up to fourth-order [9]. Spiteri and Ruuth give optimal SSP LS methods of up to third-order, some of which were found by numerical search [7].

Prior to the development of SSP methods, it was shown that the class of absolutely monotonic RK methods guaranteed non-linear stability in the sense of preserving contractivity. The most extensive study in this context is due to Kraaijevanger [10]; see also, e.g. [11–14]. Recently, it has been shown that SSP methods and absolutely monotonic methods are the same [15, 16]. This work proves that the sufficient conditions for strong stability preservation based on a representation as convex combinations of forward Euler steps are also necessary. Absolutely monotonic methods have also been shown to preserve positivity [17]. For a review of results for absolutely monotonic methods and their extension to SSP methods see [15, 18].

SSP methods are thus a key ingredient in schemes that preserve three properties of exact solutions to scalar hyperbolic conservation laws: TVD, contractivity, and positivity preservation. While *systems* of hyperbolic conservation laws do not necessarily possess these properties, numerical schemes that satisfy them in the scalar case have proven very effective when applied to systems. The TVD property is also a key element of most proofs of convergence in the non-linear scalar case, so SSP methods are important in constructing high-order convergent methods.

We have implemented conservative Godunov-type spatial discretizations of two types embedded in various time discretization procedures. The numerical flux is implemented either with a central-upwind scheme or a full Riemann flux approach. There are three components

required for updating the average state in each cell of a computational grid. First, the solution is reconstructed on cell faces from cell averages, i.e. the reconstruction stage. The second is the definition of the interface flux using the reconstructed left and right conserved values at the cell interface. The precise representation of this numerical flux is the essential difference between the central-upwind methodology and the Riemann flux method. The third component of the procedure is the time discretization, which is the focus of this paper.

Shu [5] put forth the question of 'whether it is worthwhile and necessary to use SSP time discretizations.' No answer has yet been given, except that SSP discretizations are 'at least safer.' However, he noted that 'in many situations Δt can be taken larger [than indicated by SSP theory] in practical calculations.

This paper reports on an effort to understand the importance or necessity of the SSP properties of time integration methods when used in conjunction with a conservative hyperbolic solver using either an approximate flux function methodology represented by the central-upwind methodology or an exact Riemann solver approach. We present below additional information useful for perspective on this issue. We also investigate the question of how large Δt can be taken in practice when using an SSP method. We investigate only second and third-order schemes; for some comparisons between classical and SSP fourth and fifth-order methods, see References [7, 19].

In Section 2, we describe the SSP integration concept in detail by analytically mapping the SSP properties of second and third-order RK methods in their respective parameter spaces. We also discuss a low-storage algorithm that has not been considered previously in the context of SSP methods; we present a new optimal third-order low-storage SSP method using this algorithm. In Section 3, we describe the central-upwind schemes and Riemann interface flux methodology. Finally we compare numerical results using the various spatial discretizations with SSP and non-SSP time discretizations for discontinuous non-linear hyperbolic problems.

2. SSP TIME INTEGRATION METHODS

In this section, we outline the general theory of strong-stability preserving Runge–Kutta (SSPRK) time integration methods, discuss a simple illustrative example, and describe the theory of second- and third-order SSPRK methods in detail. We also discuss two low-storage third-order families of methods and give a new optimal SSP low-storage method which improves over the optimal low storage method previously documented. Our discussion will be limited to explicit methods.

SSP methods were originally called total variation diminishing (TVD) time discretization methods because they were associated with the total variation (TV) norm,

$$\|u^n\|_{\mathrm{TV}} = \sum_j |u_j^n - u_{j-1}^n| \tag{3}$$

A time integration method is termed strongly stable in a given norm $\|\cdot\|$ under a suitable time step restriction if

$$\|u^{n+1}\| \leqslant \|u^n\| \tag{4}$$

A method that is strongly stable in the TV norm is described as TVD.

SSPRK time stepping methods provide non-linear strong stability in any norm under which a forward Euler time step is strongly stable. This property is obtained by ensuring that each stage can be represented as a convex combination of stable forward Euler steps. Recall that Runge–Kutta (RK) methods of a given order of accuracy are often left with free parameters to be chosen at will. These free parameters can be chosen, for instance, to satisfy low-storage requirements, provide an SSP property, or deliver minimal truncation error. Very unfortunate choices may also be made, yielding a poor method which is still formally of the given order of accuracy.

Any irreducible (see Reference [10] for a discussion of irreducibility) s-stage RK method may be uniquely specified by its Butcher array:

$$\begin{array}{c|ccc} c_1 & a_{11} & \cdots & a_{1s} \\ \vdots & \vdots & \ddots & \vdots \\ c_s & a_{s1} & \cdots & a_{ss} \\ \hline & b_1 & \cdots & b_s \end{array}$$

The method is then

$$u^{(i)} = u^n + \Delta t \sum_{j=1}^{s} a_{ij} \mathscr{L}(u^{(j)}) \quad (1 \leqslant i \leqslant s) \tag{5}$$

$$u^{n+1} = u^n + \Delta t \sum_{j=1}^{s} b_j \mathscr{L}(u^{(j)}) \tag{6}$$

We always assume that

$$c_i = \sum_{j=1}^{s} a_{ij} \quad (1 \leqslant i \leqslant s) \tag{7}$$

We consider only explicit methods, for which we also have

$$a_{ij} = 0 \quad (j \geqslant i) \tag{8}$$

Depending on how the coefficients are chosen the integrator may be chosen to give solutions accurate to order $p \leqslant s$.

The SSP property of an explicit s-stage Runge–Kutta scheme is most conveniently obtained by writing the scheme in the Shu–Osher [6] form

$$u^{(0)} = u^n \tag{9}$$

$$u^{(i)} = \sum_{j=0}^{i-1} (\alpha_{ij} u^{(j)} + \Delta t_{\mathrm{RK}} \beta_{ij} \mathscr{L}(u^{(j)})), \quad i = 1, \ldots, s \tag{10}$$

$$u^{n+1} = u^{(s)} \tag{11}$$

where SSP schemes have $\alpha_{ij} \geqslant 0$ and $\beta_{ij} \geqslant 0$. Since consistency requires

$$\sum_{k=0}^{i-1} \alpha_{ik} = 1 \quad (1 \leqslant i \leqslant s) \tag{12}$$

then for $\alpha_{ij}, \beta_{ij} \geqslant 0$, the method (9)–(11) is equivalent to a convex combination of forward Euler steps with step sizes $\beta_{ij}/\alpha_{ij}\Delta t_{\mathrm{RK}}$.

If we now assume that the discrete spatial operator $\mathscr{L}$ in (2) is such that (4) is satisfied for a forward Euler time step

$$u^{n+1} = u^n + \Delta t_{\mathrm{FE}} \mathscr{L}(u^n) \tag{13}$$

then the method (9)–(11) will satisfy (4) provided that

$$\Delta t_{\mathrm{RK}} \leqslant \hat{c} \Delta t_{\mathrm{FE}} \tag{14}$$

where

$$\hat{c} = \min_{i,j} \frac{\alpha_{ij}}{\beta_{ij}} \tag{15}$$

Here we may simply discard arguments to the min function for which $\beta_{ij} = 0$. The maximum over all available sets of coefficients α_{ij} and β_{ij} then gives the SSP coefficient:

$$c^{\mathrm{SSP}} = \max_{\alpha_{ij}, \beta_{ij}} (\hat{c}) \tag{16}$$

We will call c^{SSP} the SSP *coefficient* of the method. It has been referred to as the CFL *coefficient* of the method; however, it is in general not related to the CFL condition, nor does it arise from the same kind of consideration.

Note that while the Shu–Osher representation (Equations (9)–(11)) is non-unique, the SSP coefficient is unique, and can be determined from the Butcher array (in fact, it is the radius of absolute monotonicity [15, 16]). The Shu–Osher form simply allows convenient determination by inspection.

In this paper, we do not consider methods with negative coefficients, as they require an additional spatial operator in order to be SSP.

The CFL number is defined for any RK method as

$$\mathrm{CFL} = \frac{\Delta t}{\Delta x} \lambda \tag{17}$$

where λ is the local wave speed. Under the restriction

$$\mathrm{CFL} \leqslant \frac{1}{2} \tag{18}$$

some of the schemes we consider in this paper are provably TVD. We therefore define

$$\Delta t_{\mathrm{FE}} = \frac{\Delta x}{2\lambda} \tag{19}$$

An *optimal* SSP method is one for which no other method exists with the same values of s and p and a larger value of c^{SSP}. A *non-optimal* SSP method is any other method with $c^{\mathrm{SSP}} > 0$. If the above process for determining c^{SSP} yields $c^{\mathrm{SSP}} \leqslant 0$, we write $c^{\mathrm{SSP}} = 0$ and say the method is *non*-SSP.

2.1. A simple example

Two-stage, second-order RK schemes for autonomous ordinary differential equations may be written as a one-parameter family:

$$\begin{array}{c|cc} 0 & 0 & 0 \\ \frac{1}{2\gamma} & \frac{1}{2\gamma} & 0 \\ \hline & 1-\gamma & \gamma \end{array}$$

or equivalently

$$u^{(1)} = u^n + a_{21}\Delta t \mathscr{L}(u^n) \tag{20}$$

$$u^{n+1} = u^n + b_1\Delta t \mathscr{L}(u^n) + b_2\Delta t \mathscr{L}(u^{(1)}) \tag{21}$$

where

$$a_{21} = \frac{1}{2\gamma} \tag{22}$$

$$b_1 = 1-\gamma \tag{23}$$

$$b_2 = \gamma \tag{24}$$

The choice of γ affects the SSP coefficient, as well as several other properties of the method. A few examples of second-order RK methods are given in Table I. In our discussion, we will refer to methods both by the corresponding value of γ and by the names given in Table I.

Gottlieb and Shu (GS) give an example to demonstrate the importance of SSP methods [3, 4]. It involves the inviscid Burgers' equation

$$u_t + \left(\frac{1}{2}u^2\right)_x = 0 \tag{25}$$

with initial data

$$u(x,0) = \begin{cases} 1.0 & 0 < x < 0.5 \\ -0.5 & 0.5 < x < 1 \end{cases}$$

In this experiment we used the central-upwind scheme proposed in Reference [20]. We ran this simulation to time $t = 0.125$ on a grid of 1000 cells (≈ 500 time steps) using four different

Table I. Parameter values, SSP coefficients, truncation error coefficients, and empirical stability results for various second-order RK methods.

Name	γ	c^{SSP}	C_2	c^{TVD}
GS non-TVD example	$-1/40$	0	63	0
SSP22	1/2	1	2	1.0
MTE22	3/4	1/2	1	1.4
Midpoint RK2	1	0	1.5	1.4
SSP32	—	2	—	2.4
SSP42	—	3	—	2.8

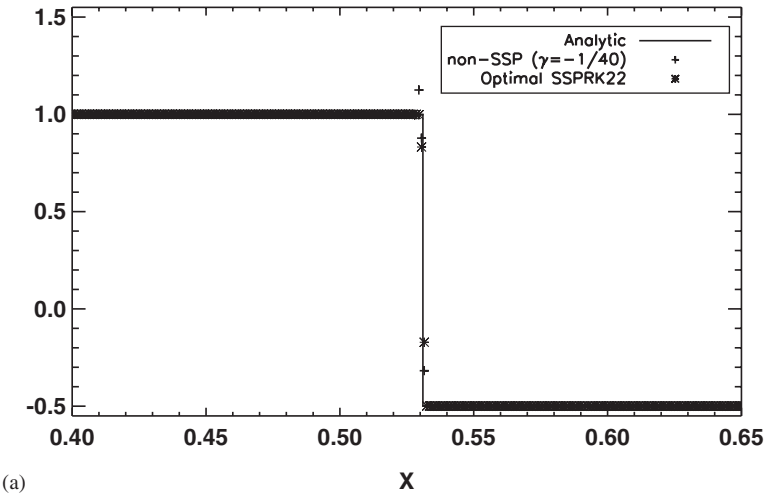

(a)

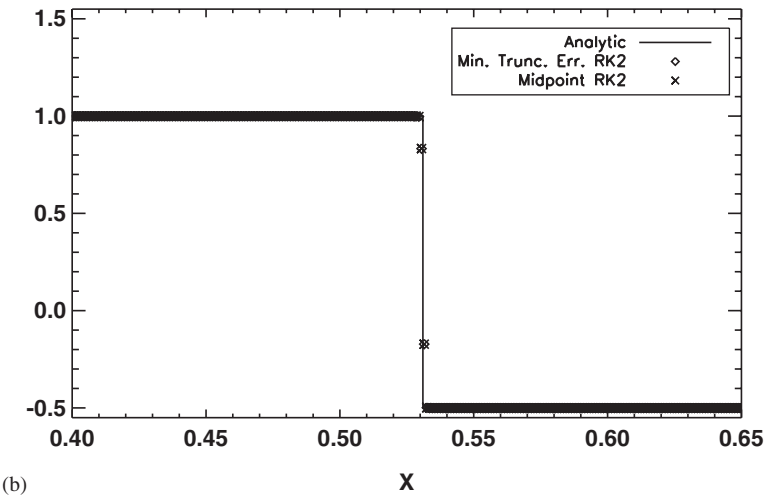

(b)

Figure 1. Solutions to Burger's equation using various SSP and non-SSP time integrators. The initial condition is a step function, which merely propagates to the right. Note that Gottlieb and Shu's example scheme produces an overshoot (top), while two commonly used methods do not (bottom): (a) Gottlieb and Shu's test; and (b) Two commonly used second-order RK methods applied to the same test.

second-order RK methods from Table I. In Figure 1(a) we reproduce the result of Gottlieb and Shu (GS) [3, 4]. The time integrators are a very poorly designed non-SSP method and an optimal SSP method (SSP22). The non-SSP method corresponds to a choice of $\gamma = \frac{-1}{40}$ which, as we shall see, is an extremely poor choice. As expected, the non-SSP method gives rise to an overshoot exactly as found by GS, while the SSP method does not. In fact, the non-SSP method becomes unstable at a CFL number slightly greater than 0.3; therefore these tests were performed at a CFL of 0.3. While this extreme example serves to demonstrate the danger of using a poor method, a comparison of more standard methods is still in order.

In Figure 1(b), we compare two commonly used RK2 methods: the (non-optimal SSP) minimal truncation error method, which is SSP at half the usual CFL, and the midpoint method, which is non-SSP. Neither of these integrators yields overshoots, even though this test employed a CFL beyond the theoretical SSP limit of either method. We calculated the total variation of the solution at each time step for each of the four methods, and with the exception of the GS non-TVD example, all integrators gave strictly TVD results.

Speaking of RK time integrators, Williamson noted that

> '...no one scheme can be superior to all others for all sets of differential equations: by a judicious choice of example any scheme could be made to appear the best' [9].

In all of our results below, standard non-optimal or non-SSP Runge–Kutta methods that are optimized for other properties, e.g. truncation error, yield comparable results to an optimal SSP time integration method.

Our intent is to provide a general perspective on the sharpness of non-linear stability limits of RK methods when applied to finite volume semi-discretizations. However, our results apply with certainty only to the specific integrators, spatial discretizations, and applications we consider here. A larger experience base is needed in order to test the generality of our findings.

2.2. Second order SSPRK methods

Table I gives the SSP stability coefficients for several second-order RK integrators outlined below. The last column of Table I, labelled c^{TVD}, is an empirical result explained in Section 4.1.1.

2.2.1. Two-stage, second order SSPRK methods. We discuss second-order RK schemes with 2 stages. These schemes can be written as a one parameter family, given by Equations (20)–(24). Given assumed constants M and L related to $\mathscr{L}$ and the time-derivatives of $\mathscr{L}$, the following error equation is obtained:

$$|\varepsilon| \leqslant \frac{h^3}{3} ML^2 C_2 \tag{26}$$

where

$$C_2 = 2\left|\frac{3}{4\gamma} - 1\right| + 1 \tag{27}$$

A minimum truncation error (MTE) scheme is obtained for $\gamma = 3/4$. Details can be found in Section 2.3 of Gear's text [21].

An SSP scheme can be written as convex combinations of Euler steps. To examine the SSP properties of a Runge–Kutta scheme we write the method as a non-unique convex combination of Euler steps (Equations (9)–(11)) and optimize on the free coefficients to find the optimal stability result. We obtain

$$\alpha_{10} = 1 \tag{28}$$

$$\beta_{10} = 1/(2\gamma) \tag{29}$$

$$\alpha_{20} = 1 - \alpha_{21} \tag{30}$$

$$\beta_{20} = 1 - \gamma - \alpha_{21}\beta_{10} \tag{31}$$

$$\beta_{21} = \gamma \tag{32}$$

The SSP coefficient is then

$$\hat{c} = \min\left(2\gamma, \frac{1-\alpha_{21}}{1-\gamma-\alpha_{21}/(2\gamma)}, \frac{\alpha_{21}}{\gamma}\right) \tag{33}$$

provided each numerator and denominator are non-negative. This leads to $0 \leqslant \gamma \leqslant 1$ and $0 \leqslant \alpha_{21} \leqslant 1$. The value of α_{21} which maximizes the terms in the minimum function of Equation (33) is

$$\alpha_{21} = 2\gamma(1-\gamma) \tag{34}$$

This clearly satisfies the requirement $0 \leqslant \alpha_{21} \leqslant 1$ for the allowable values of γ and we have

$$c^{\mathrm{SSP}} = \min(2\gamma, 2(1-\gamma)) \tag{35}$$

provided $0 \leqslant \gamma \leqslant 1$. We give several methods and their respective SSP coefficients. If $\gamma = 1/2$, then $c^{\mathrm{SSP}} = 1$ and this method is the optimal SSP second-order method. It is also known as Heun's method or the trapezoidal rule RK2 method. In terms of truncation error estimates it is clear that the GS non-TVD example is far out of normal practice for RK2 schemes. It has a truncation error coefficient 63 times larger than the optimal truncation error scheme. The optimal truncation error method is SSP stable at an SSP coefficient of 1/2 but also has a truncation error coefficient half as large as the optimal SSP method.

2.2.2. Optimal second-order SSPRK methods with additional stages. In Reference [7], Spiteri and Ruuth give a formulation for optimal s-stage, second order methods, and show that they have $c^{\mathrm{SSP}} = s - 1$. These methods were originally proposed by Kraaijevanger [10], who also proved many other results on optimal methods, in the context of contractivity. These methods are advantageous since the extra stages extend the effective stability limit. We have implemented the three- and four-stage methods.

The three-stage integrator (SSP32) is

$$\mathbf{u}^{(1)} = \mathbf{u}^n + \frac{1}{2}\Delta t \mathscr{L}(\mathbf{u}^n)$$

$$\mathbf{u}^{(2)} = \mathbf{u}^{(1)} + \frac{1}{2}\Delta t \mathscr{L}(\mathbf{u}^{(1)})$$

$$\mathbf{u}^{n+1} = \frac{1}{3}\mathbf{u}^n + \frac{2}{3}\mathbf{u}^{(2)} + \frac{1}{3}\Delta t \mathscr{L}(\mathbf{u}^{(2)})$$

which by inspection has $c^{\mathrm{SSP}} = 2$.

The four-stage method (SSP42) is

$$\mathbf{u}^{(1)} = \mathbf{u}^n + \frac{1}{3}\Delta t \mathscr{L}(\mathbf{u}^n)$$

$$\mathbf{u}^{(2)} = \mathbf{u}^{(1)} + \frac{1}{3}\Delta t \mathscr{L}(\mathbf{u}^{(1)})$$

$$\mathbf{u}^{(3)} = \mathbf{u}^{(2)} + \frac{1}{3}\Delta t \mathscr{L}(\mathbf{u}^{(2)})$$

$$\mathbf{u}^{n+1} = \frac{1}{4}\mathbf{u}^{n} + \frac{3}{4}\mathbf{u}^{(3)} + \frac{1}{4}\Delta t \mathscr{L}(\mathbf{u}^{(3)})$$

which by inspection has $c^{\mathrm{SSP}} = 3$.

2.3. Third-order RK methods

Table II gives the SSP coefficients for several third order RK integrators outlined below.

2.3.1. Three-stage, third-order SSPRK methods. Third-order RK integrators may be written as a two parameter family [22]

$$\mathbf{u}^{(1)} = \mathbf{u}^{n} + a_{21}\Delta t \mathscr{L}(\mathbf{u}^{n}) \tag{36}$$

$$\mathbf{u}^{(2)} = \mathbf{u}^{n} + a_{31}\Delta t \mathscr{L}(\mathbf{u}^{n}) + a_{32}\Delta t \mathscr{L}(\mathbf{u}^{(1)}) \tag{37}$$

$$\mathbf{u}^{n+1} = \mathbf{u}^{n} + b_1\Delta t \mathscr{L}(\mathbf{u}^{n}) + b_2\Delta t \mathscr{L}(\mathbf{u}^{(1)}) + b_3\Delta t \mathscr{L}(\mathbf{u}^{(2)}) \tag{38}$$

where a_{ij}, b_j, c_j are the ordinary Butcher array coefficients, related by

$$a_{21} = c_2 \tag{39}$$

$$a_{31} = \frac{3c_2c_3(1-c_2) - c_3^2}{c_2(2-3c_2)} \tag{40}$$

$$a_{32} = \frac{c_3(c_3 - c_2)}{c_2(2-3c_2)} \tag{41}$$

$$b_1 = 1 + \frac{2 - 3(c_2 + c_3)}{6c_2c_3} \tag{42}$$

Table II. Parameter values, SSP coefficients, truncation error coefficients, and empirical stability results for various third-order RK methods.

Name	c_2	c_3	c^{SSP}	C_3	c^{TVD}
SSP33	1	1/2	1	3.750	1.5
SSP43	—	—	2	—	2.0
MTE33	1/2	3/4	0	1.000	1.5
Optimal SSP33(2N)	0.924574	0.373462	0.322349	4.403	1.6
Optimal SSP33(2R)	0.755726	0.632124	0.838384	2.539	1.6
Williamson LS(2N)	1/3	3/4	0	1.417	1.5

$$b_2 = \frac{3c_3 - 2}{6c_2(c_3 - c_2)} \tag{43}$$

$$b_3 = \frac{2 - 3c_2}{6c_3(c_3 - c_2)} \tag{44}$$

We omit here discussion of the cases $c_3 = c_2$, $c_2 = 0$, and $c_3 = 0$, as they have already been shown to be non-SSP [3]. As in the second-order case, the SSP properties of these schemes can be computed by writing them as a (non-unique) convex combination of Euler steps (Equations (9)–(11)) and optimizing on the free parameters. We thus obtain

$$\eta_1 = \frac{1}{a_{21}} \tag{45}$$

$$\eta_2 = \min\left(\frac{1 - \alpha_{21}}{a_{31} - \alpha_{21}a_{21}}, \frac{\alpha_{21}}{a_{32}}\right) \tag{46}$$

$$\eta_3 = \min\left(\frac{1 - \alpha_{31} - \alpha_{32}}{b_1 - \alpha_{31}a_{21} - \alpha_{32}a_{31}}, \frac{\alpha_{31}}{b_2 - \alpha_{32}a_{32}}, \frac{\alpha_{32}}{b_3}\right) \tag{47}$$

$$\hat{c} = \min(\eta_1, \eta_2, \eta_3) \tag{48}$$

and in order to compute a positive SSP coefficient we impose non-negativity for the numerator and denominator of each argument in the minimum functions. This implies immediately that a_{21}, a_{32}, b_3, α_{21}, and α_{32} are non-negative. Non-negativity of $\alpha_{21}a_{21}$ in Equation (46) implies non-negativity of a_{31}. Similarly, non-negativity of $\alpha_{32}a_{32}$ in Equation (47) implies that b_2 is non-negative. Finally, non-negativity of $\alpha_{31}a_{21}$ and $\alpha_{32}a_{31}$ in Equation (47) implies that b_1 is non-negative. Thus, all of the coefficients in the Butcher array must be non-negative for methods with $c^{\mathrm{SSP}} > 0$. For a given Butcher array, the α_{ij} that maximize the values of the minimum functions may be obtained by setting the denominators with α_{ij} in them equal to zero, yielding

$$\alpha_{21} = \frac{a_{31}}{a_{21}} \tag{49}$$

$$\alpha_{31} = \frac{b_1 - b_2 a_{31}/a_{32}}{a_{21}} \tag{50}$$

$$\alpha_{32} = \frac{b_2}{a_{32}} \tag{51}$$

These choices will lead to the optimal value of c^{SSP} for the scheme, provided that they give non-negative values of all numerators and denominators in the right hand sides of Equations (45)–(47).

In this case, the final result is obtained by substituting Equations (49)–(51) into Equations (45)–(47). In terms of c_2 and c_3, we obtain

$$c^{\mathrm{SSP}} = \min\left(\frac{1}{c_2}, \frac{3c_2(1 - c_2) - c_3}{c_2(c_3 - c_2)}, \frac{3c_3 - 2}{c_3 - c_2}\right) \tag{52}$$

provided a_{ij} and b_i are non-negative. The optimal SSP case is $c_2 = 1$, $c_3 = 1/2$ in which case it is easy to show that $c = 1$.

It is possible that Equations (49)–(51) may lead to negative values of α_{31}, $1 - \alpha_{21}$, or $1 - \alpha_{31} - \alpha_{32}$. The values of c_2 and c_3 for which Equation (49) gives $1 - \alpha_{21} < 0$ also lead to negative Butcher coefficients and a non-SSP result. In the region for which Equations (50)–(51) lead to $1 - \alpha_{31} - \alpha_{32} < 0$, it is still possible to choose α_{31} and α_{32} such that $\eta_3 > \eta_2$, so that Equation (52) remains valid. Equation (50) gives $\alpha_{31} < 0$ when (c_2, c_3) is below the curve

$$c_3 = \frac{\mu}{6} - \frac{11c_2^2 - 10c_2}{6\mu} + \frac{c_2}{6} + \frac{1}{3} \tag{53}$$

where

$$\mu = \left(-17c_2^3 + 33c_2^2 - 12c_2 - 4\sqrt{1620c_2^6 - 4752c_2^5 + 4797c_2^4 - 1656c_2^3 - 120c_2^2 + 96c_2 + 16} \right)^{1/3} \tag{54}$$

In this case, one may find the optimal α_{31} and α_{32} by noting that the arguments to the min function in Equation (47) are surfaces in the $(\alpha_{31},\alpha_{32})$ parameter space. The optimal choice must lie either at a local maximum of one of the surfaces, on an intersection of two of the surfaces, or on a boundary where one of the denominators vanishes. Some computation reveals that the optimal choice in the region defined by Equation (53) may be obtained by choosing

$$\alpha_{31} = \frac{b_1 - \alpha_{32} a_{31}}{a_{21}} \tag{55}$$

so that the denominator in the first argument of Equation (47) vanishes, then determining α_{32} by setting the other two arguments equal to each other. The result is

$$\alpha_{32} = \frac{\left(18c_2c_3 - 6c_3 - 6\sqrt{-15c_3^2c_2^2 + 6c_3^2c_2 + 12c_2^2c_3 - 8c_2c_3}\right)(3c_2 - 2)}{72c_2c_3^2(c_2 - c_3)} \tag{56}$$

and c^{SSP} in this region is then given by

$$c^{\mathrm{SSP}} = \min\left(\frac{1}{c_2}, \frac{3c_2(1 - c_2) - c_3}{c_2(c_3 - c_2)}, \frac{\alpha_{32}}{b_3}\right) \tag{57}$$

This analysis is summarized in Figure 2, which is a contour plot of c^{SSP} as a function of c_2 and c_3. The optimal SSP method and the minimal truncation error method are marked, along with three low-storage methods that we describe below. The peak of the upper-left region corresponds to $c^{\mathrm{SSP}} = 0.75$, while the lower-right region peaks at $c^{\mathrm{SSP}} = 1.0$, corresponding to the optimal SSP method. No contours are plotted where $c^{\mathrm{SSP}} < 0$.

Given assumed constants M and L related to $\mathscr{L}$ and the time-derivatives of $\mathscr{L}$, the error bound for three-stage, third-order methods is [22]

$$|\varepsilon| \leqslant \frac{h^4}{24}\frac{8}{3} ML^3 C_3 \tag{58}$$

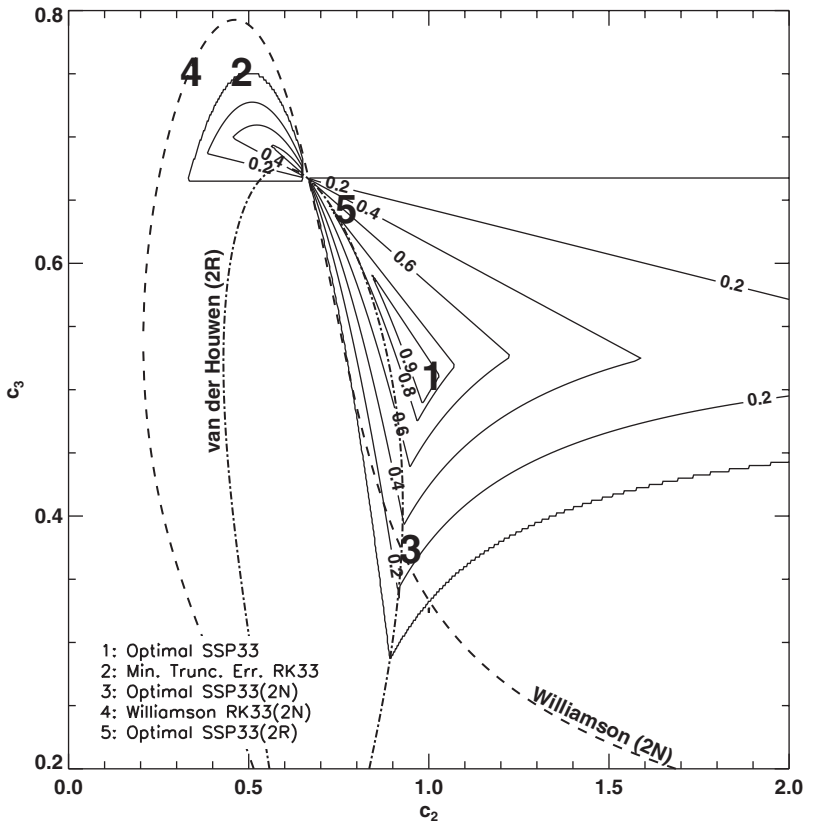

Figure 2. Contour map of theoretical SSP region for three-stage, third-order RK methods. Contour values correspond to SSP coefficients c^{SSP}. The two dashed lines indicate the 2R and 2N families of low-storage schemes. The numbers denote the locations of specific methods in parameter space. Regions without contours are non-SSP.

where

$$C_3 = |3 - 4(c_2 + c_3) + 6c_2c_3)| + \left|\frac{3}{2} - 3c_2\right| + \left|\frac{9}{2} - 6c_3\right| + \frac{3}{4} \tag{59}$$

Values of C_3 for several methods are given in Table II. The minimal truncation error RK33 method which has $c_2 = 1/2$, $c_3 = 3/4$ is non-SSP.

2.3.2. Four-stage, third-order SSPRK methods (*SSP43*). The four-stage third-order SSPRK method of Spiteri and Ruuth is

$$\mathbf{u}^{(1)} = \mathbf{u}^n + \frac{1}{2}\Delta t \mathscr{L}(\mathbf{u}^n)$$

$$\mathbf{u}^{(2)} = \mathbf{u}^{(1)} + \frac{1}{2}\Delta t \mathscr{L}(\mathbf{u}^1)$$

$$\mathbf{u}^{(3)} = \frac{2}{3}\mathbf{u}^n + \frac{1}{3}\mathbf{u}^{(2)} + \frac{1}{6}\Delta t\mathscr{L}(\mathbf{u}^{(2)})$$

$$\mathbf{u}^{n+1} = \mathbf{u}^{(3)} + \frac{1}{2}\Delta t\mathscr{L}(\mathbf{u}^{(3)})$$

which by inspection has $c^{\mathrm{SSP}} = 2$.

2.4. Low-storage third order SSPRK methods

2.4.1. Williamson (2N) methods. Williamson [9] gives a family of third-order RK schemes that may be implemented using only twice the memory needed for a single time level and is defined by

$$c_3^2(1-c_2) + c_3\left(c_2^2 + \frac{c_2}{2} - 1\right) + \left(\frac{1}{3} - \frac{c_2}{2}\right) = 0 \tag{60}$$

Such methods have been referred to as 2N methods [1]. The algorithm is

$$\begin{aligned}
\mathbf{u} &= \mathbf{u}^n \\
\Delta\mathbf{u} &= \Delta t\mathscr{L}(\mathbf{u}) \\
\mathbf{u} &= \mathbf{u} + B_1\Delta\mathbf{u} \\
\Delta\mathbf{u} &= \Delta t\mathscr{L}(\mathbf{u}) + A_2\Delta\mathbf{u} \\
\mathbf{u} &= \mathbf{u} + B_2\Delta\mathbf{u} \\
\Delta\mathbf{u} &= \Delta t\mathscr{L}(\mathbf{u}) + A_3\Delta\mathbf{u} \\
\mathbf{u}^{n+1} &= \mathbf{u} + B_3\Delta\mathbf{u}
\end{aligned}$$

where

$$B_j = a_{j+1\ j} \quad (j<3) \tag{61}$$

$$B_3 = b_3 \tag{62}$$

$$A_1 = 0 \tag{63}$$

$$A_j = \frac{a_{j+1\ j-1} - c_j}{B_j} \quad (j>1) \tag{64}$$

Again, the c_j are free parameters and the $a_{i,j}$ and b_j are given by Equations (39)–(44). Two 2N schemes are given in Table II. The Williamson LS(2N) scheme is Williamson's preferred method based on truncation error and scheme simplicity.

We have plotted in Figure 2 the branch of this family that passes through the SSP region in the (c_2, c_3) plane. The 2N curve (Equation (60)) intersects the lower-right boundary of the SSP region at the point $(0.9245741121, 0.3734617067)$, which corresponds to $c^{\mathrm{SSP}} = 0.322$. This method was previously found by numerical search [3, 7]. It is clear from

Figure 2 that this method (herein Optimal SSP33(2N)) is the optimal three-stage third-order 2N SSP method.

2.4.2. van der Houwen (2R) methods. van der Houwen (vdH) [23] gives an alternate low-storage algorithm:

$$\begin{aligned}
\mathbf{v} &= \Delta t \mathscr{L}(\mathbf{u}) \\
\mathbf{u} &= \mathbf{u} + a_{21}\mathbf{v} \\
\mathbf{v} &= \mathbf{u} + (b_1 - a_{21})\mathbf{v} \\
\mathbf{u} &= \Delta t \mathscr{L}(\mathbf{u}) \\
\mathbf{v} &= \mathbf{v} + a_{32}\mathbf{u} \\
\mathbf{u} &= \mathbf{v} + (b_2 - a_{32})\mathbf{u} \\
\mathbf{u}^{n+1} &= \mathbf{u} + b_3 \Delta t \mathscr{L}(\mathbf{v})
\end{aligned}$$

Here, a_{ij} and b_j are the Butcher coefficients of the scheme. Lambert [24] derives the following family (in the case of three-stage, third-order methods) of vdH schemes:

$$c_2 = \frac{4 - 7c_3 + 6c_3^2 \pm \sqrt{c_3^2(17 - 60c_3 + 84c_3^2 - 48c_3^3)}}{6(1 - 2c_3 + 2c_3^2)} \tag{65}$$

Such methods are referred to as 2R methods to distinguish them from Williamson's 2N methods [1]. A simple optimization using (65) and (52) shows that the optimal value of c^{SSP} for a 2R method occurs at $(0.7557263130, 0.6321247848)$ giving $c^{\mathrm{SSP}} = 0.838$, a substantial improvement over the optimal 2N method. It also has a truncation error half that of the optimal 2N method. We refer to this method as Optimal SSP33(2R). The Butcher array for this method is

0	0	0	0
0.7557263130	0.7557263130	0	0
0.6321247848	0.2451702923	0.3869544938	0
	0.2451702923	0.1848960428	0.5699336658

3. SPATIAL DISCRETIZATION

In this section we summarize the spatial discretizations used for our numerical experiments, the numerical flux methods we employ, including two approximate central-upwind fluxes and an exact Riemann flux, and the associated reconstruction methods [25]. We comment on two non-oscillatory reconstruction methods found in the literature and show by test and analysis that they are actually not third-order in general as previously claimed. Finally, we discuss total variation diminishing properties of the semi- and fully discrete schemes.

The spatial discretizations we investigate are representative of those that have been used in the SSP literature, i.e. second- and third-order TVD and ENO schemes using approximate

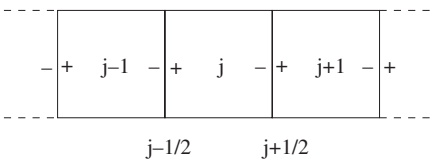

Figure 3. Grid layout for reconstruction and flux evaluation.

Riemann solvers [3, 4, 6–8]. Although the TVD semi-discrete schemes have recently been derived as central-upwind schemes, it is interesting to note that they fall into the class of generalized MUSCL schemes developed by Osher [26], who also proved that such schemes are TVD.

We evaluate the numerical flux function at states on the cell boundaries using polynomial reconstructions from cell averages. Figure 3 shows the indexing scheme and grid layout. In the methods discussed below, the reconstructed field values are located at the plus '+' and '−' locations in each cell, where + and − are associated with the right and left sides of each cell face respectively. For a given cell at grid-location j, the left face corresponds to $j-1/2$, and the right face to $j+1/2$.

The error associated with the reconstruction may be defined as the difference between the reconstructed and exact fields,

$$\mathbf{u}^e(x,t)-\mathbf{u}^r(x,\bar{\mathbf{u}})=\mathbf{O}(\Delta x^n) \tag{66}$$

where $\mathbf{u}^e$ is the exact field and $\mathbf{u}^r$ is the reconstructed field, and the cell-centered average is denoted by an over-bar. The difference between the exact and reconstructed field is $\mathbf{O}(\Delta x^n)$ for an n-order reconstruction. We only consider grids with uniform spacing in order to avoid additional complexities associated with the reconstruction methods and in performing numerical analysis. In the sections below all min, max and inequality operators acting on vectors are assumed to apply component-by-component.

3.1. Numerical flux

One-dimensional grid updates of the average conserved field variables are calculated using a conservative update as

$$\frac{\mathrm{d}}{\mathrm{d}t}\bar{\mathbf{u}}_j(t)=-\frac{\mathbf{H}_{j+1/2}-\mathbf{H}_{j-1/2}}{\Delta x} \tag{67}$$

where the numerical fluxes, $\mathbf{H}_{j\pm1/2}$, are given according to either a central or Riemann flux prescription. We use three flux methods. The first two are central scheme methods developed by Kurganov and Tadmor (KT) and Kurganov, Noelle, and Petrova (KNP) in References [20, 27]. Both flux methods rely on estimates of the minimum and maximum wave speeds at the cell interfaces, which are computed using

$$a^N_{j+1/2}=\max\left[\lambda_N\left(\frac{\partial\mathbf{f}}{\partial\mathbf{u}}\left(\mathbf{u}^-_{j+1/2}\right)\right),\lambda_N\left(\frac{\partial\mathbf{f}}{\partial\mathbf{u}}\left(\mathbf{u}^+_{j+1/2}\right)\right),0\right] \tag{68}$$

and

$$a^1_{j+1/2} = \min\left[\lambda_1\left(\frac{\partial \mathbf{f}}{\partial \mathbf{u}}\left(\mathbf{u}^-_{j+1/2}\right)\right), \lambda_1\left(\frac{\partial \mathbf{f}}{\partial \mathbf{u}}\left(\mathbf{u}^+_{j+1/2}\right)\right), 0\right] \tag{69}$$

where $\mathbf{f}$ represents one spatial component of the flux vector $\mathbf{F}_i$, λ_1 is the minimal eigenvalue of the flux Jacobian, and λ_N is the maximal eigenvalue. The one-dimensional flux updates, as described below, are compatible with a second-order reconstruction and the dimension-by-dimension third-order reconstruction methods. A genuinely multi-dimensional third-order method would require flux evaluations at cell vertices as well as at cell faces as described by Kurganov and Petrova [28]. The KT flux uses only the maximum wave speed, $a_{j+1/2} = \max(|a^N_{j+1/2}|, |a^1_{j+1/2}|)$, at the cell interfaces. The numerical flux is

$$\mathbf{H}_{j+1/2} = \frac{\mathbf{F}(\mathbf{u}^-_{j+1/2}) + \mathbf{F}(\mathbf{u}^+_{j+1/2})}{2} - \frac{a_{j+1/2}}{2}(\mathbf{u}^+_{j+1/2} - \mathbf{u}^-_{j+1/2}) \tag{70}$$

The central-upwind flux of Kurganov, Noelle and Petrova uses both maximal wave speeds, a^1 and a^N, at cell interfaces [20], i.e.

$$\mathbf{H}_{j+1/2} = \frac{a^N_{j+1/2}\mathbf{F}(\mathbf{u}^-_{j+1/2}) - a^1_{j+1/2}\mathbf{F}(\mathbf{u}^+_{j+1/2})}{a^N_{j+1/2} - a^1_{j+1/2}} + \frac{a^N_{j+1/2}a^1_{j+1/2}}{a^N_{j+1/2} - a^1_{j+1/2}}(\mathbf{u}^+_{j+1/2} - \mathbf{u}^-_{j+1/2}) \tag{71}$$

It is possible for the denominator to be zero in Equation (71) when $a^N_{j+1/2} = a^1_{j+1/2} = 0$. Our implementation checks for this pathology and uses the average of the interface fluxes in this case.

The last flux is a Riemann flux formulation where the Riemann problem using the left and right reconstructed values as left and right state is solved in order to find the vector of conserved variables, $\mathbf{u}^*_{j+1/2}$ at the interface location. The numerical flux is then simply

$$\mathbf{H}_{j+1/2} = \mathbf{F}(\mathbf{u}^*_{j+1/2}) \tag{72}$$

The Riemann flux at the interface is calculated for each face at each stage of the Runge–Kutta step.

3.2. *Reconstruction methods*

We now describe the methods used for reconstruction of values at cell boundaries, including two linear and three quadratic methods. Both of the linear reconstruction methods are second-order and use slope limiting. In both, the undivided differences are used at grid location j and $j-1$ as

$$\Delta\bar{\mathbf{u}}_j = \bar{\mathbf{u}}_{j+1} - \bar{\mathbf{u}}_j \tag{73}$$

$$\Delta\bar{\mathbf{u}}_{j-1} = \bar{\mathbf{u}}_j - \bar{\mathbf{u}}_{j-1} \tag{74}$$

From these two differences, a limited difference $\delta\mathbf{u}_j$ is determined for each cell. The reconstructed left and right values for each cell are then given by

$$\mathbf{u}^-_{j+\frac{1}{2}} = \bar{\mathbf{u}}_j + \frac{1}{2}\delta\mathbf{u}_j \tag{75}$$

$$\mathbf{u}^{+}_{j-\frac{1}{2}} = \bar{\mathbf{u}}_j - \frac{1}{2}\,\delta\mathbf{u}_j \tag{76}$$

3.2.1. Superbee. The second-order Superbee limiter is [29]

$$\delta\mathbf{u}_j = \frac{\text{sign}(\Delta\bar{\mathbf{u}}_{j-1}) + \text{sign}(\Delta\bar{\mathbf{u}}_j)}{2}\ \max(\min(2|\Delta\bar{\mathbf{u}}_{j-1}|, |\Delta\bar{\mathbf{u}}_j|), \min(|\Delta\bar{\mathbf{u}}_{j-1}|, 2|\Delta\bar{\mathbf{u}}_j|)) \tag{77}$$

3.2.2. Minmod. The second-order Minmod limiter is [29]

$$\delta\mathbf{u}_j = \frac{\text{sign}(\Delta\bar{\mathbf{u}}_{j-1}) + \text{sign}(\Delta\bar{\mathbf{u}}_j)}{2}\ \min(|\Delta\bar{\mathbf{u}}_{j-1}|, |\Delta\bar{\mathbf{u}}_j|) \tag{78}$$

3.2.3. Non-oscillatory reconstruction (LT3 & KP3). We implemented two non-oscillatory reconstruction methods, LTE and KP3, which are based on limited quadratic reconstructions (see References [30, 31] and [28], respectively). LT3 forms a convex combination of a constant and a quadratic reconstruction via a limiting parameter θ_j while KP3 implements a convex combination of a linear and a quadratic reconstruction, again via a limiting parameter θ_j. However, neither of these methods is third-order accurate in general, as will be discussed below.

3.2.4. Central weighted essentially non-oscillatory reconstruction (CWENO3). As an alternative to the LT3 and KP3 methods we implemented a third-order accurate CWENO scheme due to Levy, Puppo and Russo [32]. Similar to KP3, this method involves a convex combination of linear and quadratic reconstructions. We refer the reader to that paper for details; we use the parameter choices $C_L = C_R = \frac{1}{4}$, $\varepsilon = 10^{-4}$, and $p = 2$. This reconstruction does not satisfy conditions (91)–(92) below, and so leads to a non-TVD scheme.

3.3. Accuracy of reconstructions KP3, LT3 and CWENO3

We were able to reproduce the third-order convergence results presented in References [28, 31] for the problem of advecting a sine wave using LT3 and KP3 reconstruction. However, we observed sub-third-order convergence rates using these methods to solve Burgers' equation (Equation (25)) with initial data

$$u(x, 0) = 0.5 + \sin(x) \quad 0 < x < 2\pi \tag{79}$$

The solution was obtained at time $t = 0.5$ (before a shock develops), and convergence rates were determined by comparing the computed and exact solutions on a series of grids. That is, we compute

$$\|u_{\text{calc}} - u_{\text{exact}}\| \tag{80}$$

where $\|\cdot\|$ represents either the L_1 norm or the L_∞ norm. The results, using the KNP flux and the SSP33 time integrator are shown in Tables III and IV. Similar results were obtained using the other flux functions.

With CWENO3 we were able to recover high accuracy on the smooth Burger's equation test problem. The super-convergent results are consistent with results obtained in Reference [32].

Table III. L^1 errors and estimated order of convergence for solutions to Burgers equation at $t = 0.5$ (pre-shock).

	CWENO3		LT3		KP3	
Cells	L^1	Order	L^1	Order	L^1	Order
128.	7.146E-04	—	5.909E-05	—	5.189E-05	—
256.	1.133E-04	2.657	8.057E-06	2.875	9.682E-06	2.422
512.	1.665E-05	2.767	1.073E-06	2.909	4.408E-06	1.135
1024.	1.775E-06	3.230	1.448E-07	2.890	1.442E-06	1.612
2048.	1.382E-07	3.682	2.081E-08	2.798	4.012E-07	1.846
4096.	9.136E-09	3.919	3.972E-09	2.389	1.057E-07	1.925
8192.	5.702E-10	4.002	8.386E-10	2.244	2.913E-08	1.859
16384.	3.561E-11	4.001	1.884E-10	2.154	7.954E-09	1.873

Table IV. L^∞ errors and estimated order of convergence for solutions to Burgers equation at $t = 0.5$ (pre-shock).

	CWENO3		LT3		KP3	
Cells	L^∞	Order	L^∞	Order	L^∞	Order
128.	7.875E-04	—	1.290E-04	—	1.341E-04	—
256.	9.991E-05	2.979	2.656E-05	2.280	5.753E-05	1.221
512.	1.984E-05	2.332	5.651E-06	2.233	4.047E-05	0.507
1024.	2.689E-06	2.883	1.216E-06	2.217	1.895E-05	1.095
2048.	2.359E-07	3.511	2.550E-07	2.253	8.772E-06	1.111
4096.	1.628E-08	3.857	5.564E-08	2.196	3.845E-06	1.190
8192.	1.039E-09	3.970	1.183E-08	2.234	1.944E-06	0.984
16384.	6.631E-11	3.970	2.513E-09	2.235	9.405E-07	1.048

Sub-third-order convergence results were obtained for LT3 and KP3. The results for LT3 reconstruction are consistent with those presented for this problem in References [30, 31], where the sub-third-order convergence was not explained.

We discovered that the procedures used to compute the limiting parameters θ_j, as documented, are deficient and that the order of accuracy may actually be much less than claimed for smooth problems. Below we document flaws in the limited reconstruction procedures. The orders of accuracy discussed below are consistent with the numerical results shown in Tables III and IV.

The deterioration of the LT3 scheme has already been discussed by Bianco, Puppo and Russo who show that if θ_j is not regular enough accuracy will deteriorate [33]. Our approach is to directly calculate the expected order of accuracy of θ_j.

The key failure in the proof that LT3 is third-order on smooth data is in the estimate for θ_j. It is required that the θ_j values used in each cell satisfy $\theta_j = 1 + O(h^3)$ as h approaches zero. If both the left and right sides of the cell satisfy this condition then the cell as a whole will satisfy it. The quantities M_j and $M_{j+1/2}$ are different quadratic reconstructions for $\mathbf{u}(x_{j+1/2})$. It is true that $M_{j+1/2} - M_j$ is $O(h^3)$ ([31, p. 407]). However, it is the θ_j values from the left or right-hand side of each cell which are used in the reconstruction and these must be at most

$O(h^3)$ away from 1. A typical formula for θ_j is

$$\theta_j = \frac{M_{j+1/2} - \overline{\mathbf{u}}_j}{M_j - \overline{\mathbf{u}}_j} \tag{81}$$

Since we are using quadratic reconstructions, the values at the cells edges can be represented as

$$\theta_j \sim \frac{\mathbf{u}(x_{j+1/2}) + \varepsilon_1 h^3 - \overline{\mathbf{u}}_j}{\mathbf{u}(x_{j+1/2}) + \varepsilon_2 h^3 - \overline{\mathbf{u}}_j} \tag{82}$$

as h approaches 0. Now $\varepsilon_1 \neq \varepsilon_2$ in general since the reconstructed third-order point values feeding into the formula come from different data sets. Then we obtain

$$\theta_j \sim 1 + \frac{\varepsilon_1 - \varepsilon_2}{\mathbf{u}(x_{j+1/2}) - \overline{\mathbf{u}}_j} h^3 \tag{83}$$

and estimating further

$$\theta_j \sim 1 + 2\frac{\varepsilon_1 - \varepsilon_2}{\mathrm{d}\mathbf{u}/\mathrm{d}x(x_j)} h^2 \tag{84}$$

Thus in general θ_j may be $O(h^2)$ away from 1. Thus LT3 cannot be expected to be better than second-order accurate.

Now let us examine a typical formula for θ_j used in the left/right estimate minimization procedure for KP3 ([28, p. 694]):

$$\theta_j = \frac{M_{j+1/2} - L_{j+1/2}}{M_j - L_{j+1/2}} \tag{85}$$

Here the $L_{j+1/2}$ are linear reconstructions. Since the M_j and $M_{j+1/2}$ are again quadratic reconstructions in smooth regions, the values at the cell edges can be represented as

$$\theta_j \sim \frac{\mathbf{u}(x_{j+1/2}) + \varepsilon_1 h^3 - (\mathbf{u}(x_{j+1/2}) + \varepsilon_3 h^2)}{\mathbf{u}(x_{j+1/2}) + \varepsilon_2 h^3 - (\mathbf{u}(x_{j+1/2}) + \varepsilon_3 h^2)} \tag{86}$$

as h approaches 0. Now $\varepsilon_1 \neq \varepsilon_2$ in general since the reconstructed third-order point values feeding into the formula come from different data sets. Then we obtain

$$\theta_j \sim 1 + \frac{\varepsilon_1 - \varepsilon_2}{\varepsilon_3} h \tag{87}$$

In general θ_j may be $O(h)$ away from 1. Thus KP3 cannot be expected to be better than first-order accurate.

3.4. The TVD property

In solving Equation (1) with $\mathbf{u}$ a scalar, total variation diminishing schemes are desirable because the exact solution is TVD. When (1) represents a system of equations, this is not generally true; however, the application of a TVD scheme tends to avoid the creation of spurious oscillations near discontinuities, an undesirable tendency of high-order schemes. In this section we discuss the conditions under which the schemes we have presented are provably TVD. In our discussion we make an important distinction between a semi-discrete TVD property and the TVD property for a fully discrete scheme.

3.4.1. Semi-discrete TVD schemes. In this section we discuss conditions on $\mathscr{L}$ such that the solution to (2) satisfies

$$\|\mathbf{u}(\cdot,t)\|_{\mathrm{TV}} \leqslant \|\mathbf{u}(\cdot,0)\|_{\mathrm{TV}} \tag{88}$$

In this case we say that the semi-discrete scheme (2) is TVD.

Tadmor [34] gives the following conditions for generalized MUSCL schemes to possess a TVD property. Slightly more restrictive conditions were given by Osher [26]. Such schemes require that the numerical flux, $\mathbf{H}_{j+1/2}(\mathbf{u}^-_{j+1/2}, \mathbf{u}^+_{j+1/2})$, satisfy

$$\mathrm{sign}(\mathbf{u}_{j+1} - \mathbf{u}_j) \cdot (\mathbf{H}_{j+1/2}(\mathbf{u}_j, \mathbf{u}_{j+1}) - \mathbf{F}(\mathbf{u})) \leqslant 0 \tag{89}$$

for $\min(\mathbf{u}_j, \mathbf{u}_{j+1}) \leqslant \mathbf{u} \leqslant \max(\mathbf{u}_j, \mathbf{u}_{j+1})$. Here $\mathbf{F}$ is the physical flux function defined in (1). Both fluxes (70) and (71) satisfy this condition, as does the exact Riemann flux.

The scheme will then be TVD if two requirements on the reconstructed values are met. The first is that

$$\mathbf{u}^+_{j-1/2} = \mathbf{u}^-_{j+1/2} = \mathbf{u}_j \tag{90}$$

when $\mathbf{u}_j$ is an extremum of the solution. The second is

$$\mathrm{sign}(\mathbf{u}_{j+1} - \mathbf{u}_j) = \mathrm{sign}(\mathbf{u}_{j+1} - \mathbf{u}^-_{j+1/2}) \tag{91}$$

$$\mathrm{sign}(\mathbf{u}_j - \mathbf{u}_{j-1}) = \mathrm{sign}(\mathbf{u}_j - \mathbf{u}^-_{j-1/2}) \tag{92}$$

Both Superbee and Minmod reconstruction satisfy these conditions, so combining either of them with any of our proposed fluxes results in a TVD semi-discrete scheme.

The LT3 and KP3 reconstructions guarantee the non-oscillatory property

$$\mathrm{sign}(\mathbf{u}_{j+1} - \mathbf{u}_j) = \mathrm{sign}(\mathbf{u}^+_{j+1/2} - \mathbf{u}^-_{j+1/2}) \tag{93}$$

$$\mathrm{sign}(\mathbf{u}_j - \mathbf{u}_{j-1}) = \mathrm{sign}(\mathbf{u}^+_{j-1/2} - \mathbf{u}^-_{j-1/2}) \tag{94}$$

This implies the weaker condition (91)–(92). They also satisfy (90).

We are unaware of a third-order reconstruction that satisfies (90)–(92). We remark that methods have so far been sought (e.g. LT3 and KP3) to satisfy (90) and (93)–(94), which is in general more restrictive. Consideration of conditions (90)–(92) may more easily lead to the formulation of a genuinely third-order reconstruction that yields a TVD semi-discrete scheme, that is, a third-order extension of Osher's second-order generalized MUSCL schemes.

3.4.2. Fully discrete TVD schemes. We are interested in schemes that are TVD under forward Euler time integration. Given such a scheme, SSP time integration will also yield a TVD discretization. The semi-discrete TVD property mentioned above only guarantees TVD in the limit as the time step approaches zero. A fully discrete TVD scheme is more difficult to obtain [34].

Consider a scheme using either Minmod or Superbee reconstruction and KT or KNP flux, combined with forward Euler time integration. Using a proof similar to that of Reference [27, Theorem 5.1], it is easy to show that such a scheme is stable and TVD under the restriction

CFL $\leqslant \frac{1}{4}$. However, this seems to be excessively restrictive; non-oscillatory results for non-linear systems of equations have been obtained with these schemes using a CFL number slightly less than $\frac{1}{2}$ [20, 35, 36]. It is possible to show that, for the linear scalar case (i.e. linear advection), KT flux yields a TVD scheme for CFL numbers less than $\frac{1}{2}$ (using Superbee) or $\frac{2}{3}$ (using Minmod).

Minmod reconstruction combined with the Riemann flux yields the semi-discretization used by Gottlieb and Shu [3]. As stated there, it is easily shown that this scheme combined with forward Euler integration is TVD up to a CFL number of $\frac{1}{2}$.

4. NUMERICAL COMPARISONS

We wish to investigate empirically the importance of using SSP time integration. Our results will shed light on the practical TVD limits of our semi-discrete schemes as well. For hyperbolic problems, SSP time integration has been deemed most important in the case of non-linear discontinuous solutions. We have therefore chosen two non-linear discontinuous test problems.

4.1. Practical strong stability regions for Burgers' equation

In this section we investigate further results for the problem in Section 2.1. Recall that the problem involves the solution to Burgers' equation with Riemann initial data. Thus, the numerical solution may be prone to develop undesirable oscillations. We desire that the total variation of the solution be non-increasing in time; this has been shown for the second-order spatial discretizations we employ when combined with forward Euler time integration (cf. Section 3.4). Therefore, any growth in the TV norm must be due to the lack of strong stability preservation in a given time integrator.

For both second- and third-order methods, a separate test was made for each variation in time step. We define the time step via a parameter c so that

$$\Delta t = c\Delta t_{\mathrm{FE}} \tag{95}$$

where Δt_{FE} is defined by Equation (19). Therefore, c is exactly twice the CFL number, which is convenient because $c = 1$ corresponds to both the largest theoretical TVD limit for any of our schemes and the CFL number near which most numerical experiments in the literature have been run [20, 35, 36]. The value of c and the parameter(s) in the RK formulation were varied over a wide range. The value

$$\max_n \left(\mathrm{TV}(u^n) - (\mathrm{TV}(u_0)\right) \tag{96}$$

giving the maximum increase in total variation over all time steps, was calculated. In this manner the region of stability was found; any result larger than roundoff error ($\approx 10^{-10}$) indicates a violation of the TVD property (instability), while a smaller result indicates stability. In order to obtain a fair comparison between schemes with different numbers of stages, we employ the effective CFL number, defined in Reference [7] as

$$c\,\frac{s^*}{s} \tag{97}$$

where c is defined by Equation (95), s is the number of stages, and s^* is the minimum number of stages required for an explicit RK method to achieve order p. For $p = 2, 3$ we have $s^* = p$.

4.1.1. Second-order results. The practical region of stability for each combination of the three flux methods and two limiters is plotted in Figures 4 and 5. Figure 4(a), using Minmod reconstruction and the exact Riemann flux, corresponds to the semi-discretization used by Gottlieb and Shu in their SSP-motivating example. This figure thus shows the results of applying the family of two-stage, second-order methods to their test. The white line represents c^{SSP}, the strict theoretical strong stability limit given that this scheme is provably TVD up to a CFL number of $\frac{1}{2}$ using forward Euler integration. For the remaining semi-discretizations, we plot the same theoretical region for reference.

While our results confirm the stability properties predicted by theory, it is immediately clear that the practical stability region extends well beyond that bound in most cases. Using SSP22 integration, little or no oscillation is introduced for $c < 2$, or equivalently, $\mathrm{CFL} < 1$. Hundsdorfer [37] noted that this is not surprising, since the first-order upwind

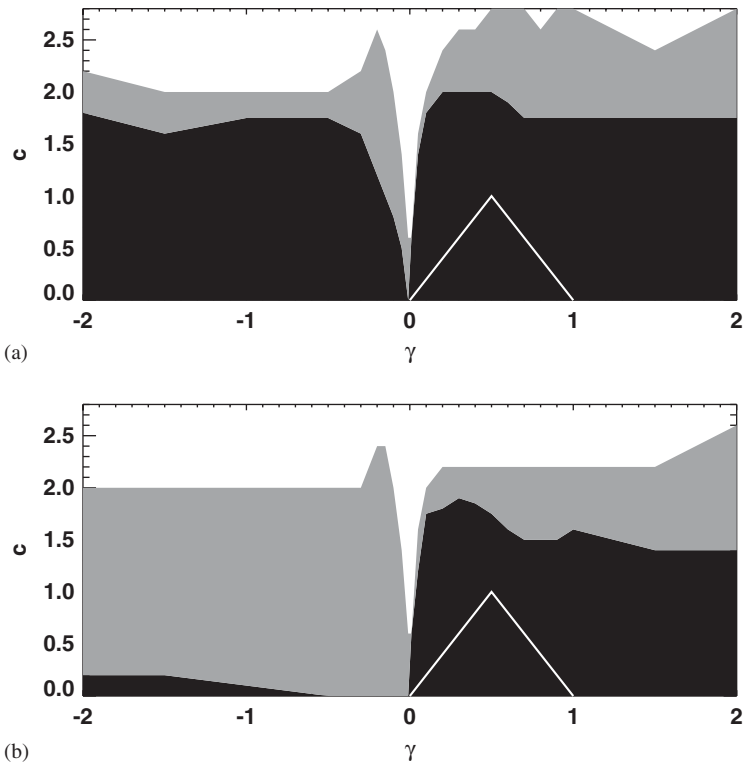

Figure 4. TV stability regions for second-order RK methods using a Riemann flux. Black represents the region of observed strong stability, grey the region of observed bounded stability, and white the region of instability: (a) TV stability regions using Minmod reconstruction and Riemann flux; and (b)TV stability regions using Superbee reconstruction and Riemann flux.

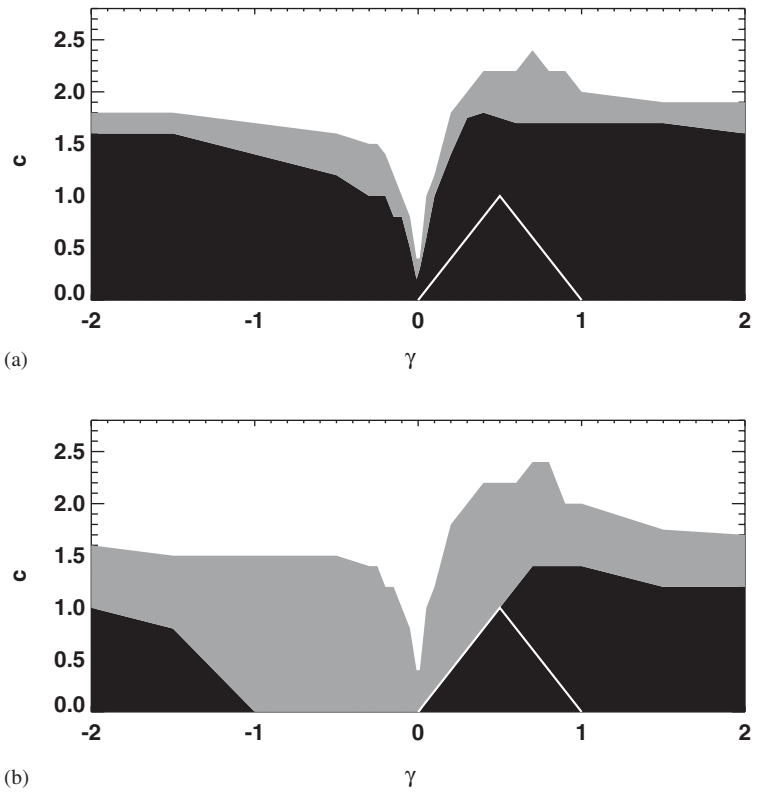

Figure 5. TV stability regions for second-order RK methods using the Kurganov–Tadmor flux. Black represents the region of observed strong stability, grey the region of observed bounded stability, and white the region of instability: (a) TV stability regions using Minmod reconstruction and KT flux; and (b) TV stability regions using Superbee reconstruction and KT flux.

method is TVD up to this limit and our schemes become close to first-order upwinding near discontinuities.

The integrator which has been used to promote the use of optimal SSP methods employs a value of $\gamma = \frac{-1}{40}$ corresponding to an extremely poor choice. Note that the intermediate step for this method is calculated at a time equivalent to twenty Euler steps backward! In general, our results show that methods with intermediate steps that severely violate the CFL condition (i.e. those with $|\frac{1}{2\gamma}| \gg 1$) perform poorly, while all methods with intermediate steps that conform to the CFL condition (those with $0 < 1/2\gamma \leqslant 1$) perform nearly as well to slightly better than the optimal SSP method for this problem. In Table I we list the empirical parameter c^{TVD}, the minimum over the set of flux functions and reconstruction combinations tested of the maximum c for which a TVD result is obtained. Since $c^{\mathrm{TVD}} p/s = 1.6$ for SSP32 and $c^{\mathrm{TVD}} p/s = 1.4$ for SSP42, it is interesting that, in this sense and for this problem, we can rank order by stability characteristics with SSP32 the best, followed by the group MTE22, midpoint RK2 and SSP42, and the optimal SSP22 coming in last!

Another point of interest is the effect of the reconstruction method on TV stability. We have used both the most and least dissipative second order TVD reconstruction (Minmod and

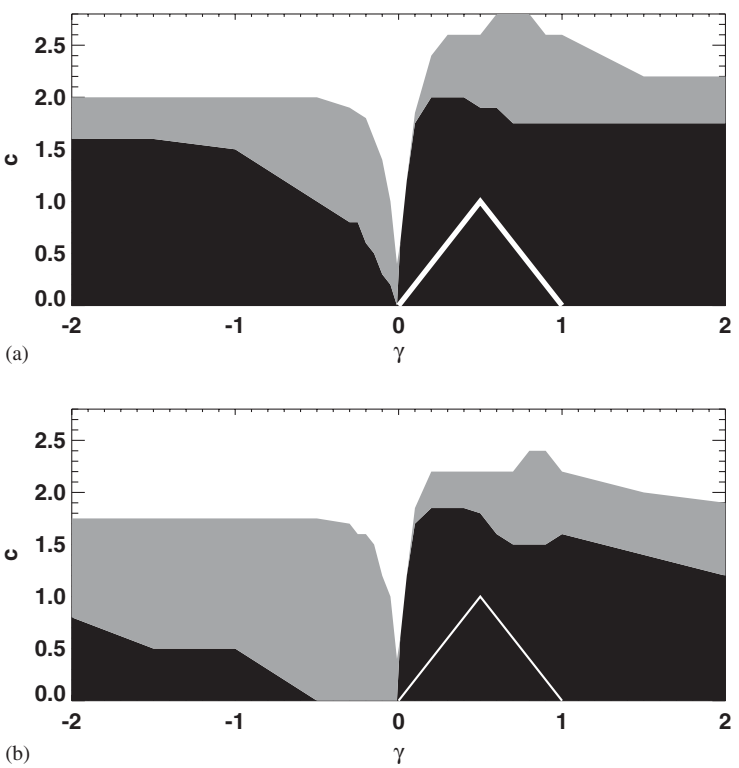

Figure 6. TV stability regions for second-order RK methods using the Kurganov–Noelle–Petrova flux. Black represents the region of observed strong stability, grey the region of observed bounded stability, and white the region of instability: (a) TV stability regions using Minmod reconstruction and KNP flux; and (b) TV stability regions using Superbee reconstruction and KNP flux.

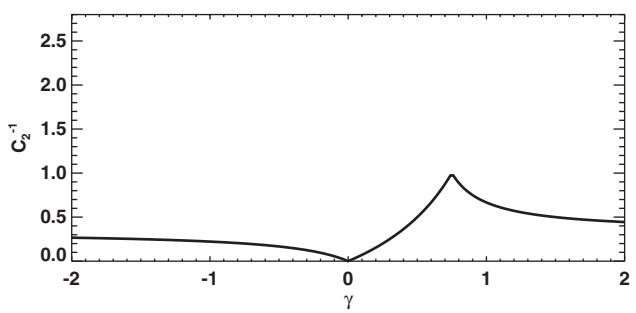

Figure 7. Reciprocal of truncation error coefficient versus γ for RK2 methods. Notice the correlation with observed stability (compare Figures 4, 5 and 6).

Superbee, respectively). The dissipation added via Minmod reconstruction apparently interacts with the SSP property, resulting in stability at higher values of c than possible using Superbee reconstruction (Figure 6).

In Figure 7 we plot $1/C_2$ versus γ, showing that the non-linear stability appears to correlate inversely with truncation error.

4.1.2. Third-order results. As mentioned in Section 3.4, we were unable to find a suitable third-order reconstruction in order to achieve a TVD semi-discrete scheme. The CWENO3 reconstruction was observed to violate the TVD property for even the smallest time steps. For this experiment, we therefore used second-order reconstruction methods.

The theoretical stability region is plotted in Figure 2; the observed TVD region is shown in Figures 8 and 9 for KNP flux combined with Minmod and Superbee reconstruction, respectively. In each plot, we indicate the various methods discussed earlier.

In contrast to the relatively small peak indicated by SSP theory, we observe TVD results throughout a large region that includes all of the well-designed methods we have considered. In both cases, all of these methods perform equally well, regardless of their values of c^{SSP}. The optimal SSP33(2R) method seems to be a good compromise between optimizing c^{SSP},

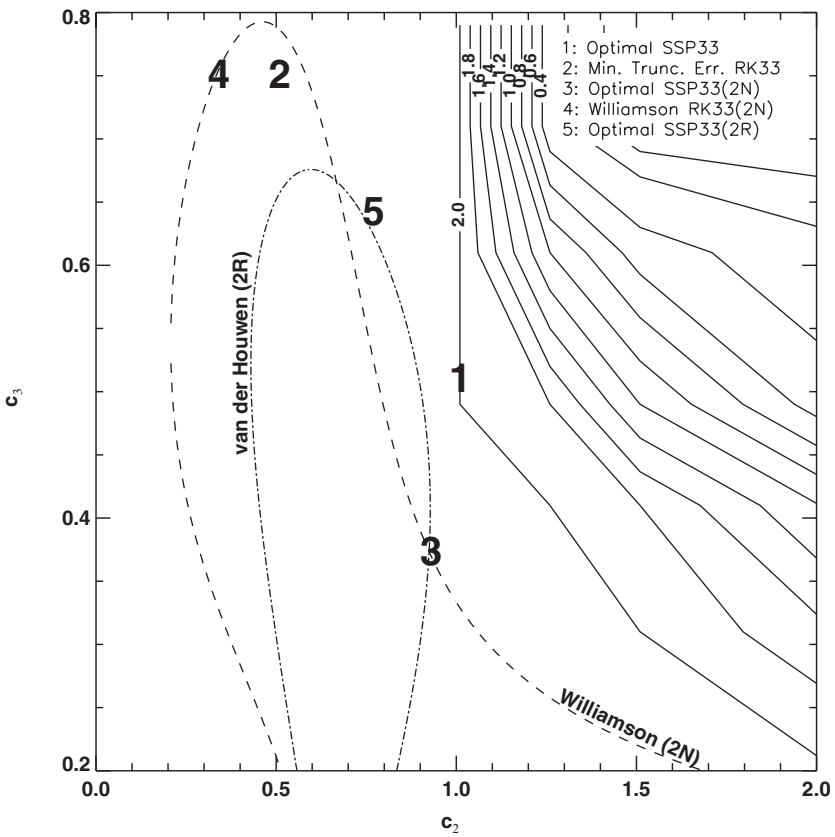

Figure 8. Contour map of observed TVD region for three-stage, third-order RK methods with Minmod/KNP. Contour values correspond to the maximum CFL coefficient for which strong stability is observed. The two dashed lines indicate the 2R and 2N families of low-storage schemes. The large numbers denote the locations of specific methods in parameter space.

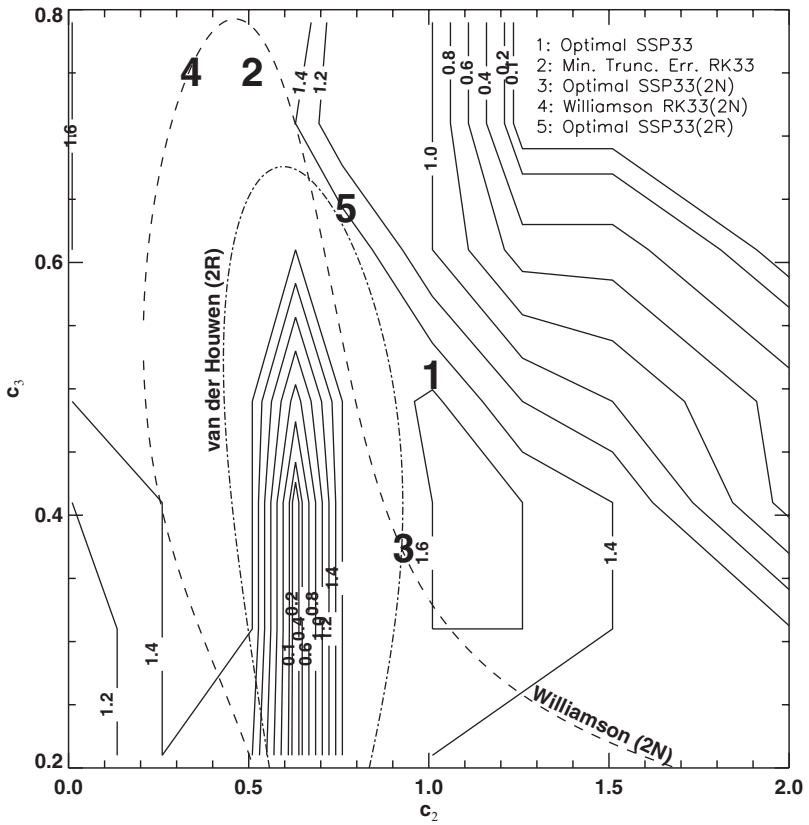

Figure 9. Contour map of observed TVD region for three-stage, third-order RK methods with Superbee/KNP. Contour values correspond to the maximum CFL coefficient for which strong stability is observed. The two dashed lines indicate the 2R and 2N families of low-storage schemes. The large numbers denote the locations of specific methods in parameter space.

the truncation error coefficient, and the memory usage. In Table II we give the empirical parameter c^{TVD}, the minimum over the set of flux functions and reconstruction combinations tested of the maximum c for which a TVD result is obtained for this problem. We observe that in this specific restricted sense the optimal low storage schemes outperform all the other third order schemes since $c^{\mathrm{TVD}}\, p/s = 1.5$ for SSP43.

In Figure 10 we plot $1/C_3$ versus γ, showing that the non-linear stability again appears to correlate inversely with truncation error, though not as strongly as in the second-order case.

4.2. Practical strong stability regions for the Euler equations

While much insight may be gained via analysis or simple numerical tests, the value of any numerical technique is ultimately determined by its performance in solving the types of problems for which it is intended. We therefore tested our suite of SSP and non-SSP methods on the Sod shocktube problem, which involves the Euler equations with discontinous initial

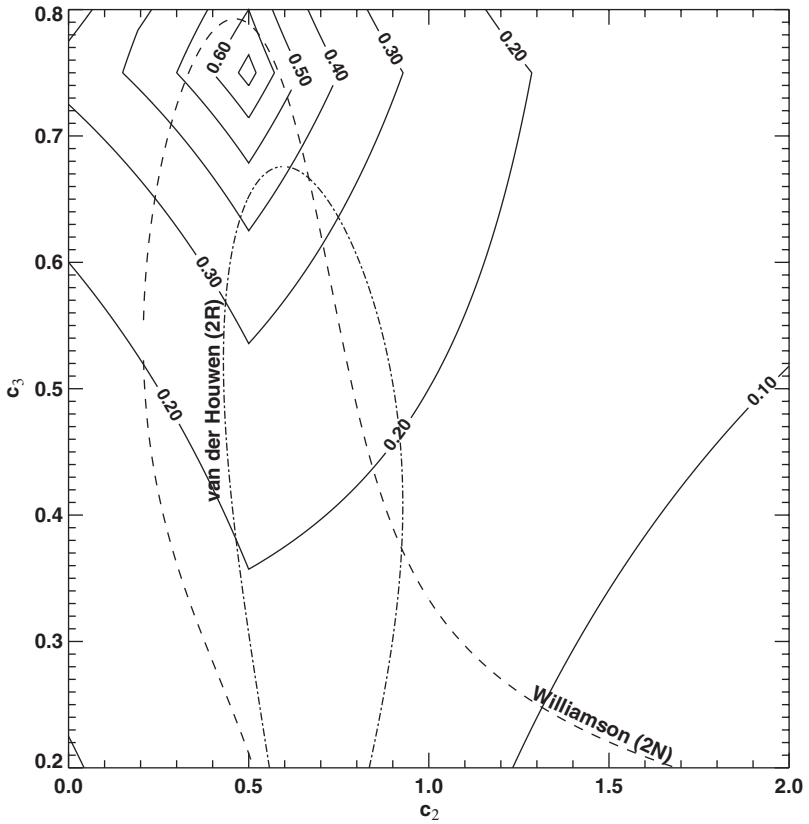

Figure 10. Contour plot of reciprocal of truncation error coefficient for three-stage, third-order RK methods. The dashed lines indicate the 2R and 2N families of low-storage schemes.

conditions. In one dimensions, the Euler equations are

$$\frac{\partial}{\partial t}\begin{Bmatrix}\rho\\ \rho u\\ E\end{Bmatrix}+\frac{\partial}{\partial x}\begin{Bmatrix}\rho u\\ \rho u^2+p\\ u(E+p)\end{Bmatrix}=0 \tag{98}$$

The initial conditions for our test problem are

$$\rho_l = 1.0$$

$$p_l = 1.0 \tag{99}$$

$$u_l = 0.0 \tag{100}$$

for the left-state (l), and

$$\rho_r = 0.125$$

$$p_r = 0.1 \tag{101}$$

$$u_r = 0.0 \tag{102}$$

for the right state. The one-dimensional domain is $0.5 < x < 1.5$, with the interface between left and right states at $x = 1$. We consider the solution on a grid of 256 cells at time $t = 0.1644$. In our discussion we refer to the TV norm, defined by Equation (3), and the L_1 norm, defined by

$$\|\mathbf{u}\|_1 = \sum_j |u_j| \tag{103}$$

4.2.1. Second-order results. Figure 11 shows the TV norm of the final density solution minus the TV at time zero versus effective CFL number for several second-order methods. No method

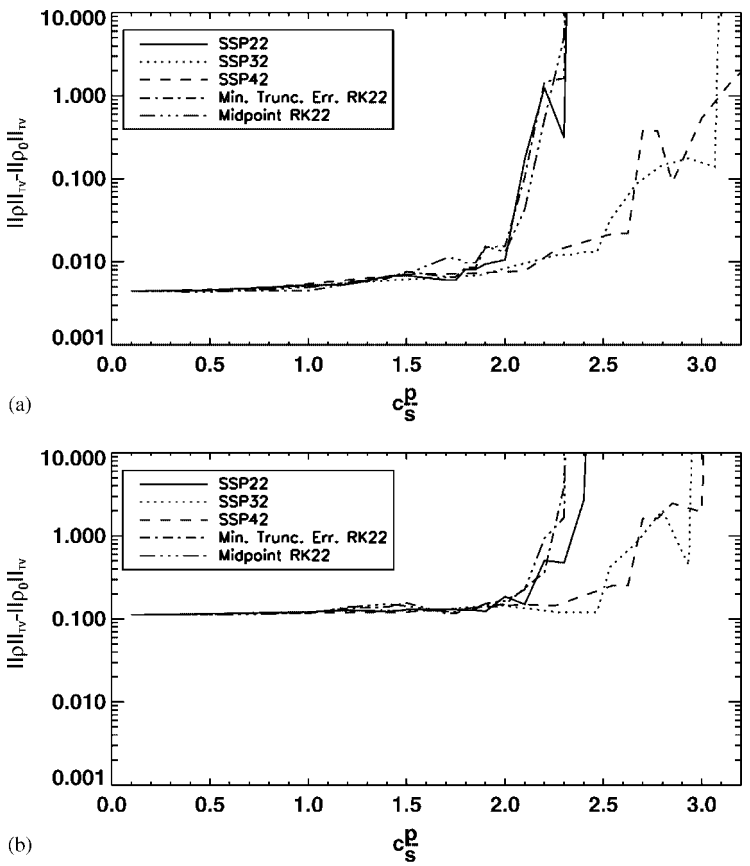

Figure 11. Results from the Sod shocktube problem, showing increase in total variation of the density solution as a function of effective CFL number for various second-order methods and two reconstruction options. Note that all results are positive, meaning that no method achieves a strictly SSP result: (a) Minmod/KNP; and (b) Superbee/KNP.

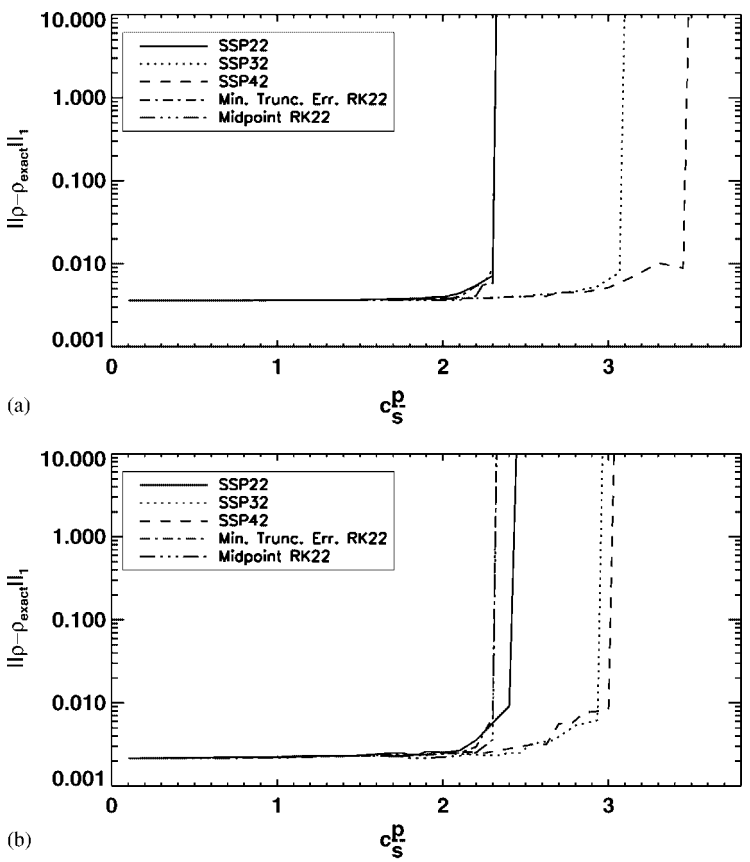

Figure 12. Results from the Sod shocktube problem, showing L_1 error in density solution as a function of effective CFL number for various second-order methods and two reconstruction options. Note the similarity of results for all methods and reasonable CFL numbers: (a) Minmod/KNP; and (b) Superbee/KNP.

achieves a TVD result at any c. This is due to the spatial discretizations, which guarantee the TVD property only in the scalar case. The three two-stage methods, which include an optimal SSP, non-optimal SSP, and non-SSP method, perform similarly, although the SSP22 method remains stable at slightly higher CFL numbers when Superbee limiting is used. In all three cases, the TV increase is small (and indistinguishable) when the CFL condition is satisfied, i.e. $c \leqslant 1$. The methods with extra stages give the expected enhanced stability properties.

In Figure 12, we examine the stability of each method. For this test, we use KNP numerical flux. The final density solution is compared to the analytic solution and the L^1 norm of the difference is plotted versus effective CFL number. The results are similar to those for Burgers' equation; well-designed non-SSP and non-optimal SSP methods perform quite similarly to the optimal SSP method. The SSPRK methods with extra stages seem to behave as expected, providing stability up to larger effective CFL numbers. Specifically, the method with one extra stage remains stable at an effective CFL number of 1.33, and the method with two

extra stages remains stable at an effective CFL number of 1.5. Figure 12 shows the stability of the various time integrators vs. time step. It is clear that there is a significant benefit to using the $s > p$ integrators which improve the effective CFL number significantly above 1/2, verifying the work of Spiteri and Ruuth [7]. Note that roughly speaking the methods begin to fail completely for values of $c\,p/s$ near $2c^{\mathrm{SSP}}\,p/s$.

4.2.2. Third-order results. This test used CWENO3 reconstruction and KNP numerical flux. Results using the Riemann flux were very similar. Figure 13(a) shows the TV norm of the final density solution minus the TV norm at time zero versus effective CFL number for several third-order methods. Again, no method achieves a TVD result at any effective CFL number, because we are now dealing with a system of equations. The three-stage methods are indistinguishable for $c \leqslant 1$, regardless of their values of c^{SSP}, including low-storage methods.

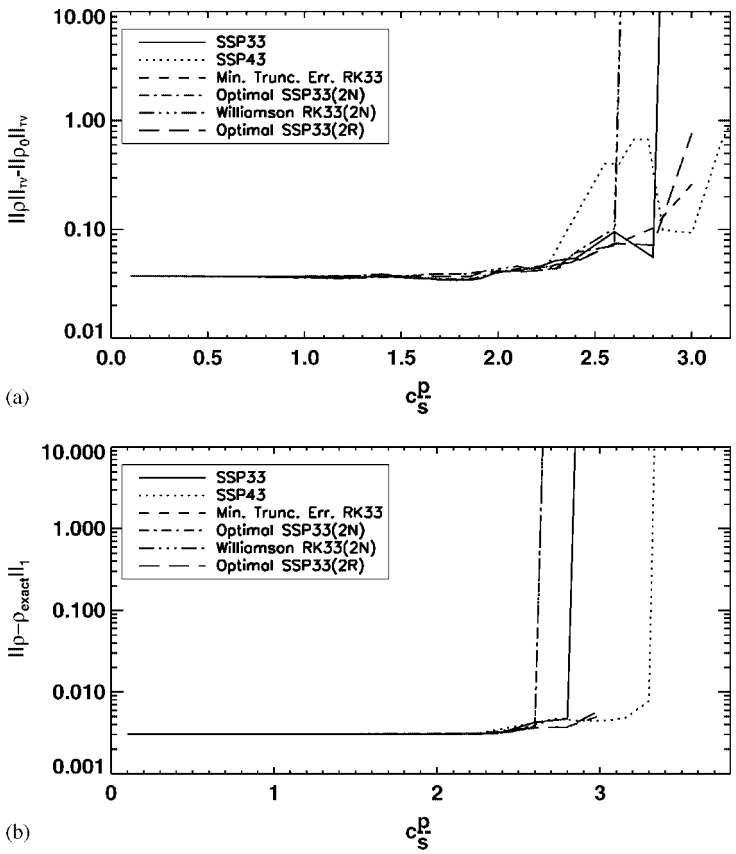

Figure 13. Stability of various third order methods versus effective CFL number on the shocktube problem: (a) Results from the Sod shocktube problem, showing increase in total variation of the density solution as a function of c for various third-order methods. Note that all results are positive, meaning that no method achieves a strictly SSP result; and (b) Results from the Sod shocktube problem, showing L_1 error in density solution as a function of effective CFL number for various third-order methods. Note the similarity of results for all methods and reasonable CFL numbers.

Figure 13(b) shows the L^1 norm of the density error. All the integrators give similar results for $c \leqslant 1$. The SSP43 scheme provides enhanced stability as expected with $c^{\mathrm{SSP}} p/s = 3/2$.

5. CONCLUSIONS

We have investigated empirically the preservation of the TVD property for Godunov-type semi-discretizations using second and third-order families of Runge–Kutta time integrators. The performance of SSP, non-optimal SSP and well designed non-SSP schemes appear to be every similar for the problems and numerical methods that we have investigated. Specifically, all three types of schemes appear to perform well in the sense of strong stability in the TV norm in all instances where the time step is maintained below the standard physical CFL limit. Further studies involving additional semi-discretizations and consideration of preservation of other stability or boundedness properties would be useful in testing the generality of this observation. A significant dependence on the reconstruction method interacting with the time integrator is noted, particularly for time integrators far from the parameter space of commonly used methods, and for CFL numbers beyond the stable limit. In addition, we have shown that second- and third-order SSP methods with $s > p$ clearly provide a useful enhanced stability region, as predicted by the analysis. The optimal SSP33(2R) method provides third-order accuracy and low storage with a significant improvement in both SSP coefficient and truncation error coefficient versus the optimal (2N) SSP low-storage method.

ACKNOWLEDGEMENTS

We acknowledge the important contributions of Mark A. Christon to the development and documentation of the conservation law code capability associated with this work [25]. The NEVADA code framework developed at Sandia National Laboratories provides the baseline software infrastructure. We wish to thank David L. Ropp for a careful review of an early draft of this paper and the reviewers for their insightful and helpful comments.

Sandia is a multiprogram laboratory operated by Sandia Corporation, a Lockheed Martin Company, for the United States Department of Energy's National Nuclear Security Administration under contract DE-AC04-94AL85000.

REFERENCES

1. Kennedy CA, Carpenter MH, Lewis RM. Low-storage, explicit Runge–Kutta schemes for compressible Navier–Stokes equations. *Applied Numerical Mathematics* 2000; **35**:177–219.
2. Kennnedy CA, Carpenter MH. Additive Runge–Kutta schemes for convection–diffusion–reaction equations. *Applied Numerical Mathematics* 2002; **44**:139–181.
3. Gottlieb S, Shu C-W. Total variation diminishing Runge–Kutta schemes. *Mathematics of Computation* 1998; **67**:73–85.
4. Gottlieb S, Shu C-W, Tadmor E. Strong stability-preserving high-order time discretization methods. *SIAM Review* 2001; **43**:89–112.
5. Shu C-W. A survey of strong stabilty preserving high order time discretizations. In *Collected Lectures on the Preservation of Stability under Discretization*, Estep D, Tavener S (eds). SIAM: Philadelphia, PA, 2002.
6. Shu C-W, Osher S. Efficient implementation of essentially non-oscillatory shock-capturing schemes. *Journal of Computational Physics* 1988; **77**:439–471.
7. Spiteri RJ, Ruuth SJ. A new class of optimal high-order strong-stability-preserving time discretization methods. *SIAM Journal on Numerical Analysis* 2002; **40**:469–491.
8. Spiteri RJ, Ruuth SJ. Nonlinear evolution using optimal fourth-order strong-stability-preserving Runge–Kutta methods. *Mathematics and Computers in Simulations* 2003; **62**:125–135.

9. Williamson JH. Low-storage Runge–Kutta schemes. *Journal of Computational Physics* 1980; **35**:48–56.
10. Kraaijevanger JFBM. Contractivity of Runge–Kutta methods. *BIT* 1991; **31**:482–528.
11. Kraaijevanger JFBM. Absolute monotonicity of polynomials occurring in the numerical solution of initial value problems. *Numerische Mathematik* 1986; **48**:303–322.
12. Kraaijevanger JFBM, Spijker MN. Algebraic stability and error propagation in Runge–Kutta methods. *Applied Numerical Mathematics* 1989; **5**:71–87.
13. Spijker MN. Contractivity in the numerical solution of initial value problems. *Numerische Mathematik* 1983; **42**:271–290.
14. Van de Griend J, Kraaijevanger JFBM. Absolute monotonicity of rational functions occurring in the numerical solution of initial value problems. *Numerische Mathematik* 1986; **49**:413–424.
15. Ketcheson DI. An algebraic characterization of strong stability preserving Runge–Kutta schemes. *Undergraduate Thesis*, Brigham Young University, 2004.
16. Ferracina L, Spijker MN. Stepsize restrictions for the total-variation-diminishing property in general Runge–Kutta methods. *SIAM Journal on Numerical Analysis* 2004; **42**:1073–1093.
17. Horvath Z. Positivity of Runge–Kutta and diagonally split Runge–Kutta methods. *Applied Numerical Mathematics* 1998; **28**:309–326.
18. Higueras I. On strong stability preserving time discretization methods. *Journal of Scientific Computing* 2004; **21**:193–223.
19. Ruuth SJ, Spiteri RJ. High-order strong-stability-preserving Runge–Kutta methods with downwind spatial discretizations. *SIAM Journal on Numerical Analysis* 2004; **42**:974–996.
20. Kurganov A, Noelle S, Petrova G. Semidiscrete central-upwind schemes for hyperbolic conservation laws and Hamilton–Jacobi equations. *SIAM Journal on Scientific Computing* 2001; **23**:707–740.
21. Gear CW. *Numerical Initial Value Problems in Ordinary Differential Equations*. Prentice-Hall: Englewoods Cliffs, NJ, 1971.
22. Ralston A, Rabinowitz P. *A First Course in Numerical Analysis*. McGraw-Hill: New York, 1978.
23. Van der Houwen PJ. Explicit Runge–Kutta formulas with increased stability boundaries. *Numerische Mathematik* 1972; **20**:149–164.
24. Lambert JD. *Numerical Methods for Ordinary Differential Systems*. Wiley: Chichester, 1991.
25. Christon MA, Ketcheson DI, Robinson AC. An assessment of semi-discrete central schemes for hyperbolic conservation laws. *Technical Report SAND03-3238*. Sandia National Laboratories: Albuquerque, New Mexico, September 2003.
26. Osher S. Convergence of generalized MUSCL schemes. *SIAM Journal on Numerical Analysis* 1985; **22**:947–961.
27. Kurganov A, Tadmor E. New high resolution central schemes for nonlinear conservation laws and convection–diffusion equations. *Journal of Computational Physics* 2000; **160**:241–282.
28. Kurganov A, Petrova G. A third-order semi-discrete genuinely multidimensional central scheme for hyperbolic conservation laws and related problems. *Numerische Mathematik* 2001; **88**:683–729.
29. LeVeque RJ. *Numerical Methods for Conservation Laws*. Birkhauser Verlag: Basel, 1992.
30. Liu X-D, Osher S. Nonoscillatory high order accurate self similar maximum principle satisfying shock capturing schemes. *I. SINUM* 1996; **33**:760–779.
31. Liu X-D, Tadmor E. Third order nonoscillatory central scheme for hyperbolic conservation laws. *Numerische Mathematik* 1998; **79**:397–425.
32. Levy D, Puppo G, Russo G. Compact central WENO schemes for multidimensional conservation laws. *SIAM Journal on Scientific Computing* 2000; **22**:656–672.
33. Bianco F, Puppo G, Russo G. High-order central schemes for hyperbolic systems of conservation laws. *SIAM Journal on Scientific Computing* 1999; **21**:294–322.
34. Tadmor E. Convenient total variation diminishing conditions for nonlinear difference schemes. *SIAM Journal on Numerical Analysis* 1988; **25**:1002–1014.
35. Kurganov A, Petrova G. Central schemes and contact discontinuities. *Mathematical Modelling and Numerical Analysis* 2000; **34**:1259–1275.
36. Kurganov A, Tadmor E. Solution of two-dimensional Riemann problems for gas dynamics without Riemann problem solvers. *Numerical Methods for Partial Differential Equations* 2002; **18**:584–608.
37. Hundsdorfer W, Ruuth SJ, Spiteri RJ. Monotonicity-preserving linear multistep methods. *SIAM Journal on Numerical Analysis* 2003; **41**:605–623.

